

## Research paper

# Investigation on the influence of temperature in L-ascorbic acid determination using FTIR-ATR terahertz spectroscopy Calibration model with temperature compensation

Meinilwita Yulia <sup>a, b</sup>, Diding Suhandy <sup>c, \*</sup>, Yuichi Ogawa <sup>a</sup>, Naoshi Kondo <sup>a</sup><sup>a</sup> Bio-Sensing Engineering (BISE) Laboratory, Graduate School of Agriculture, Kyoto University, Kitashirakawa Oiwakecho Sakyo-ku, Kyoto 606-8502, Japan<sup>b</sup> Department of Agricultural Technology, Lampung State Polytechnic, Jl. Soekarno Hatta No. 10, Rajabasa Bandar Lampung, Lampung, Indonesia<sup>c</sup> Department of Agricultural Engineering, Lampung University, Jl. Soemantri Brojonegoro No. 1, Gedongmeneng Bandar Lampung, Lampung, Indonesia

## ARTICLE INFO

## Article history:

Available online 23 August 2014

## Keywords:

Local calibration model  
 Global calibration model  
 FTIR-ATR terahertz spectroscopy  
 Temperature compensation  
 L-Ascorbic acid

## ABSTRACT

The influence of sample temperature variation on L-AA determination using Fourier transform infrared attenuated total reflectance terahertz (FTIR-ATR-THz) spectroscopy was investigated. Using the best local calibration models at 22, 31 and 40 °C, prediction results for a prediction sample set at any one temperature were excellent, with low RMSEP and high SDR<sub>pred</sub> values. However, bias and SEP were significantly increased when samples from different temperatures were used in these models; higher RMSEPs resulted. On the other hand, global calibration models based on combinations of different temperatures gave better prediction results, with lower RMSEP and higher SDR<sub>pred</sub> values for all prediction samples at 22, 31 and 40 °C. With these global calibration models the bias predictions were also significantly decreased; resulting in lower RMSEP values.

© 2014, Asian Agricultural and Biological Engineering Association. Published by Elsevier B.V. All rights reserved.

## 1. Introduction

In fruit juice production, near infrared (NIR) and mid infrared (MIR) spectroscopy using an attenuated total reflectance (ATR) sample presentation mode have been used extensively for quality inspection of products from raw materials through to final products. Currently, these techniques are being used in fruit juice analysis to determine components, such as sugar and acid content (Lanza and Li, 1984; Cen et al., 2006; Duarte et al., 2002); measure quality parameters, such as Brix and acid ratio; and to identify biological contaminants (Al-Qadiri et al., 2006; Al-Holy et al., 2006). They are also very useful in detecting the adulteration of fruit juices (Kelly and Downey, 2005; Leon et al., 2005).

However, NIR and MIR spectroscopy techniques are not suitable for inspecting packaged fruit juices, since the light from these techniques cannot pass through the packaging material. A significant disadvantage, since during transportation and storage changes in the quality of the fruit juice can occur. For instance, Burdurlu et al. (2006) reported that the vitamin C content of orange, lemon, grapefruit and tangerine decreased after eight weeks of

storage. It is also known that at higher storage temperatures (45 °C), the rate of vitamin C loss is higher than that at lower temperatures (28 °C). Even over a shorter period of several days and at lower storage temperatures, Ros-Chumillas et al. (2007) have reported that the ascorbic acid content of orange juice in PET and glass bottles (stored at 4 °C and 25 °C) decreased. For this reason, it is very important to develop a new bio-sensing method that can monitor nondestructively throughout the supply chain, the vitamin C or L-ascorbic acid (L-AA) content, and other components of the juice (without the need to open the packaged juice); an important step towards establishing a total quality management system for food quality and safety control that will benefit both producers and customers.

In this regard, terahertz (THz) spectroscopy uses low frequency electromagnetic waves which are able to penetrate many non-polar materials, such as paper, and which use low photon energy; and hence are safe for biological sensing (Jepsen et al., 2008). These characteristics may be suitable to develop a nondestructive, quality monitoring method for the juice inside packaged products in the future. Initial research has established nondestructive sensing of solutions in plastic or bottle containers using THz spectroscopy (Ikeda et al., 2005; Jepsen et al., 2008). Other instances include: Ikeda et al. (2005) who used THz-TDS (time domain spectroscopy)

\* Corresponding author.

E-mail address: [diding2004@yahoo.com](mailto:diding2004@yahoo.com) (D. Suhandy).

in transmittance mode to classify some inflammable liquids and water inside common plastic beverage bottles; and Jepsen et al. (2008) who used a reflectance mode with THz-TDS to acquire spectral information about the alcohol content inside PET (*polyethylene terephthalate*) and glass bottle containers. They also reported that it is possible to calculate the concentration of alcohol inside containers.

Recently, Suhandy et al. (2012b) developed a calibration model for L-AA determination using broad spectrum THz spectroscopy (20–450  $\text{cm}^{-1}$ ), without a temperature controller. They reported being able to measure L-AA concentration with an acceptable RMSEP of 2.79% and an RPD of 4.48. However, in the THz region where the absorbance of water is highly dependent on temperature, the spectra of any L-AA solution will also be highly dependent on the temperature of the solution (Yada et al., 2008; Rønne et al., 1997, 1999; Rønne and Keiding, 2002; Zelsmann, 1995). Therefore, to develop a more robust calibration model that could be used for L-AA determination using THz spectroscopy of products in the supply chain where wide temperature variations may be encountered, there is a need to evaluate the influence of sample temperature variations on model performance.

Several methods have been established for developing calibration models that can compensate for sample temperature variations; the objective of the current study. One method uses various selection techniques to choose specific wavelengths that are insensitive to temperature variations (Centner et al., 1996; Wülfert et al., 2000; Swierenga et al., 2000). The drawback with this method is that it is possible to exclude important wavelengths which are highly correlated to the specific target (such as L-AA) but sensitive to temperature. A second common approach is to include temperature variation in the calibration model both explicitly and implicitly. In implicit approach, a global calibration model is developed in combination with calibration samples from a broad range of temperatures (Peirs et al., 2003; Wülfert et al., 1998; Kawano et al., 1995). By doing so, it is possible to include all possible wavelengths for optimal determination of the target. However, this method requires a large data set. In this study, the implicit method was used to develop and evaluate a robust calibration model for L-AA determination in the THz region.

## 2. Materials and methods

### 2.1. L-Ascorbic acid (L-AA) solution

In this research, 52 samples of L-ascorbic acid (L-AA) solution were prepared. L-AA powder (Wako Pure Chemical Industries, Ltd., Japan) was used to make the L-AA solutions, by dissolving the powder in distilled water. The solutions were stirred well with a mixer (Tube Mixer TRIO HM-, AS ONE, Japan). The concentration range of the L-AA solutions was 0–21% (mass/mass the (w/w)). For FTIR-ATR-THz measurements, a 300  $\mu\text{L}$  sample of the L-AA solution was pipetted quickly onto the surface of the silicon prism using a micro pipette.

### 2.2. Spectral data acquisition of L-AA using FTIR-ATR-THz spectroscopy

FTIR-ATR-THz spectra of the L-AA solutions were obtained in the range 20–450  $\text{cm}^{-1}$ , using an FTIR-ATR-THz based spectrometer equipped with a temperature controller (FARIS-1S, JASCO Co., Tokyo, Japan) (Fig. 1). A 200 W high-pressure mercury lamp (Ushio, Tokyo, Japan) at room temperature was used as the light source and a pyroelectric sensor made from deuterated L-alanine triglycine sulfate (DLATGS) was used as the detector. The ATR method was

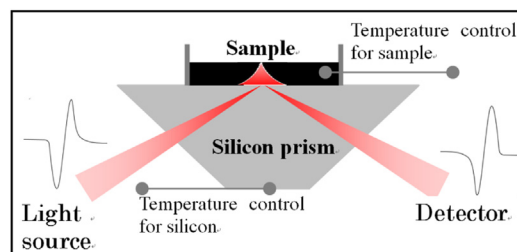


Fig. 1. ATR sample presentation mode using silicon prism equipped with temperature controller.

used for sample presentation, as described by Suhandy et al. (2012a).

Before measurement, the whole system was put under vacuum, and all spectral measurements conducted under a 150 Pa (air pressure) vacuum. Spectral acquisition parameters were as follows: 16  $\text{cm}^{-1}$  of resolution, and 200 scanning of spectral averaging. The reference for air was measured every 3 samples. For each sample, three spectral measurements were taken at the three different temperatures: 22, 31 and 40  $^{\circ}\text{C}$ , respectively. At each temperature, the spectra of 52 samples were measured. To adjust sample temperature, the temperature of the silicon prism was controlled at 24, 40 and 55  $^{\circ}\text{C}$ , respectively. The spectral intensity of the samples and reference were obtained with a single beam (SB) unit. During THz spectral measurement, room temperature and relative humidity were maintained at around 22  $^{\circ}\text{C}$  and 35%, respectively. The absorbance value of the sample was calculated using equation (1) (Suhandy et al., 2012a).

$$A(\nu) = -\log_{10} \frac{S(\nu)}{R(\nu)} \quad (1)$$

where

$A(\nu)$  is absorbance at wavenumber  $\nu$   
 $S(\nu)$  is intensity of sample at wavenumber  $\nu$   
 $R(\nu)$  is intensity of reference at wavenumber  $\nu$

One feature of ATR spectra is that ATR intensities decreased at higher wavenumber if compared to transmittance spectra (longer wavelength corresponding with greater penetration depth). For this reason, the ATR absorbance is higher at longer wavelengths or lower wavenumbers. The ATR correction accounts for this variation in effective sample path length by scaling the ATR spectrum accordingly. Most FTIR software packages, including Spectra Manager (JASCO Co., Tokyo, Japan) used in the present study incorporates an ATR correction algorithm. Suhandy et al. (2012b) used the ATR correction function provided in the software (JASCO Spectral Manager, JASCO Co., Tokyo, Japan). An alternative method to correct the ATR spectrum was used by Ogawa et al. (2009). In the present study we followed Ogawa et al. (2009) method for ATR correction by dividing the absorbance of ATR before correction with the wavelength (in micrometer). The corrected absorbance then was used for further multivariate data analysis.

### 2.3. Developing local and global calibration models using full spectrum PLS regression (FS-PLSR)

At each temperature, the 52 samples were divided into two groups; a calibration and cross-validation sample set (CalValset), and a prediction sample set (Predset). The calibration and cross-validation sample set consisted of 35 samples. This sample set was used for developing the calibration model and performing the

full cross-validation test for the local calibration model. An uncombined prediction sample set, consisting of 17 samples at each temperature, was used for prediction purposes. For the combined calibration sample set, the calibration sample sets at each temperature were combined; resulting in 70 samples for each calibration of the temperature combinations (22 and 31 °C, 22 and 40 °C, 31 and 40 °C) and 105 samples for the calibration of the temperature combination (22, 31 and 40 °C). This set was used for developing a calibration model and performing the full cross-validation test and is referred to as the global calibration model (see Fig. 2). The local and global calibration models were developed using full spectrum partial least squares regression (FS-PLSR) with full cross-validation. In FS-PLSR, the full spectrum of spectral variables and concentration data were simultaneously decomposed to a small number of latent variables, referred to as LVs or PLS factors. The first few PLS factors usually account for most of the spectra and concentration variance. Therefore, it is generally enough to obtain a satisfactory calibration and validation result by only using the first few PLS factors to establish the model. In this study, FS-PLSR models with 1–20 PLS factors were investigated, and the optimum number of PLS factors determined for use in FS-PLSR by the lowest value of the root mean square error of cross-validation (RMSECV). FS-PLSR was performed using multivariate analysis software: The Unscrambler v. 9.2 (Camo Process AS, Oslo, Norway).

Table 1 shows the statistical properties of the sample sets in detail, and the range of l-AA concentrations in the calibration and cross-validation, which cover the range in the prediction set.

2.4. Calibration model and prediction evaluation

The calibration model was evaluated based on the following parameters: number of PLS factors, coefficient of determination ( $R^2_{cal}$ ), the RMSECV, and the standard deviation ratio (SDR) of calibration ( $SDR_{cv}$ ) which can be calculated as follows (Golic and Walsh, 2006):

$$SDR_{cv} = \frac{S.D._{calibrationset}}{RMSECV} \tag{2}$$

A low RMSECV, a high  $R^2_{cal}$  and  $SDR_{cv}$  are desirable. While an  $SDR_{cv}$  above 3.0 is considered to be acceptable for practical spectroscopy applications (Clement et al., 2008).

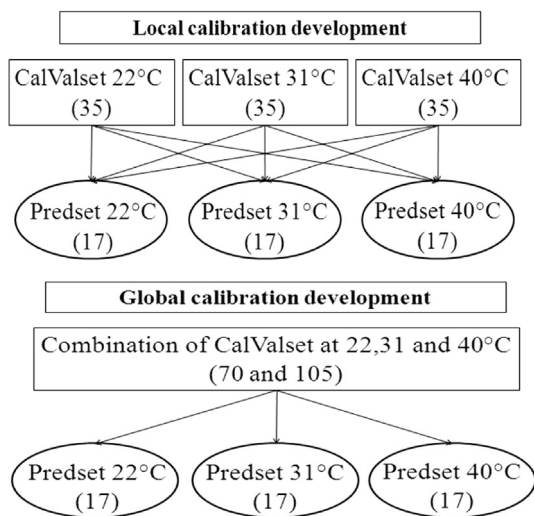


Fig. 2. Development of calibration model and prediction for uncombined and combined sample sets. The calibration models are presented in within squares while, the prediction sets are presented in the circles. The numbers of calibration and prediction sample sets are shown in the brackets.

Table 1 Characteristics of uncombined and combined samples set used for developing calibration and validation model and for prediction of l-AA determination in 22, 31 and 40 °C.

Items	Calibration and validation set	Prediction set
<b>Uncombined samples at 22, 31 and 40 °C</b>		
Samples	35	17
Range	1.4414–21.3150	2.5586–21.2575
Mean	11.53432	11.81985
S.D.	6.038385	5.975844
<b>Combined samples at 22, 31 and 40 °C</b>		
Samples	105	51
Range	1.4414–21.3150	2.5586–21.2575
Mean	11.53432	11.81985
S.D.	5.980041	5.855108
<b>Combined samples at 22 and 31, 22 and 40, 31 and 40 °C</b>		
Samples	70	34
Range	1.4414–21.3150	2.5586–21.2575
Mean	11.53432	11.81985
S.D.	5.994469	5.884605

S.D. is standard deviation of sample set. l-AA is expressed as %(mass/mass).

To evaluate the prediction performance of the developed calibration model, the following parameters were used: the coefficient of determination in prediction ( $R^2_{pred}$ ), the root mean square error of prediction (RMSEP), bias between the actual and predicted value, the bias-corrected standard error of prediction (SEP) and the standard deviation ratio (SDR) of prediction ( $SDR_{pred}$ ). The RMSEP is an estimate of total prediction errors for an independent data set. The sources of error in the RMSEP value, including bias and SEP, can be mathematically expressed as follows (Sørensen and Dalsgaard, 2005):

$$RMSEP^2 \approx SEP^2 + bias^2 \tag{3}$$

A good prediction will result in a low RMSEP, bias and SEP, and a high  $SDR_{pred}$  value. A  $SDR_{pred}$  of more than 3 is considered to be sufficient. The  $SDR_{pred}$  can be calculated as follows (Golic and Walsh, 2006; Valente et al., 2009; Liu et al., 2010):

$$SDR_{pred} = \frac{S.D._{predictionset}}{RMSECV} \tag{4}$$

3. Results and discussion

3.1. Typical spectra of l-AA at different temperatures

Fig. 3 shows the typical spectra of l-AA at 22, 31 and 40 °C, respectively. The peak was located at around 173  $cm^{-1}$  (5.2 THz). This corresponds to the intermolecular stretching vibration mode

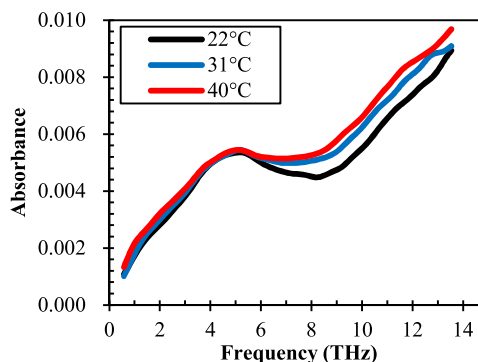


Fig. 3. A typical spectra of l-AA in aqueous solution with different temperature measured by using FTIR-ATR-THz spectroscopy in the range 0.5–13.5 THz.

**Table 2**

Local calibration results for L-AA determination using uncombined calibration sets at 22, 31 and 40 °C.

Uncombined	F <sup>a</sup>	R <sup>2</sup> <sub>cal</sub>	RMSEC	RMSECV	SDR <sub>cv</sub>
22 °C	4	0.978	0.892	1.132	5.334
31 °C	4	0.968	1.045	1.361	4.437
40 °C	3	0.964	1.131	1.339	4.512

<sup>a</sup> F is number of factor or latent variable used in the model.

of water at 5 THz (Yada et al., 2008). In general, an increasing absorbance of L-AA was observed with increasing temperature. In the lower frequencies (20–175 cm<sup>-1</sup> or 0.5–5.25 THz) the absorbance spectral difference was smaller compared to that at higher frequencies (175–450 cm<sup>-1</sup> or 5.25–13.5 THz). A similar result was also observed by Zelsmann (1995).

At lower frequencies, temperature dependence was observed, which corresponds to the temperature dependence of the slow and fast relaxation mode of water (Rønne and Keiding, 2002). No spectral differences at the peak were observed. This is thought to be related to lower temperature dependence of the stretching vibration mode of water. Very high temperature dependence was observed at higher frequencies and corresponds to the tail of the libration mode of water. The peak of the libration mode of water is located at around 15 THz and is highly temperature dependent, resulting in larger spectral differences compared to that at lower frequencies (Yada et al., 2008), as seen in Fig. 3.

### 3.2. Developing a local calibration model without temperature compensation using original and pre-processing spectra

A local calibration model for L-AA determination was developed at each sample temperature (22 °C, 31 °C and 40 °C) with original

**Table 3**

Global calibration results for L-AA determination using combined calibration sets at 22, 31 and 40 °C.

Combined	F	R <sup>2</sup> <sub>cal</sub>	RMSEC	RMSECV	SDR <sub>cv</sub>
22 and 31 °C	5	0.960	1.1929	1.3635	4.396
22 and 40 °C	5	0.960	1.1774	1.3371	4.483
31 and 40 °C	4	0.947	1.3709	1.5242	3.933
22, 31 and 40 °C	5	0.954	1.2745	1.3890	4.305

and pre-processed spectra. The best pre-processed spectra were obtained with Savitzky–Golay (SG) smoothing for 9 segments. Table 2 shows the result for the best local calibration models at 22, 31 and 40 °C, respectively.

All the best local calibration models at 22, 31 and 40 °C were of very good quality: a high R<sup>2</sup><sub>cal</sub> and a low RMSECV. The SDR<sub>cv</sub> value was also more than 3 for all local calibration models (Table 2). A plot of PLS factors versus RMSECV and a scatter plot of the best local calibration model for L-AA determination at 22, 31 and 40 °C are depicted in Fig. 4. Based on Fig. 4, the optimal number of PLS factor was 4, 4, and 3 for the local calibration model at 22, 31 and 40 °C, respectively.

### 3.3. Developing a global calibration model with temperature compensation using original and pre-processed spectra

Using a combined calibration sample set of the 22, 31 and 40 °C temperature measurements (with two and three combinations), global calibration models with 70 and 105 samples were developed with full-cross validation for original and pre-processed spectra. The global calibration model was developed to evaluate the effect of combining samples measured at different temperatures on the

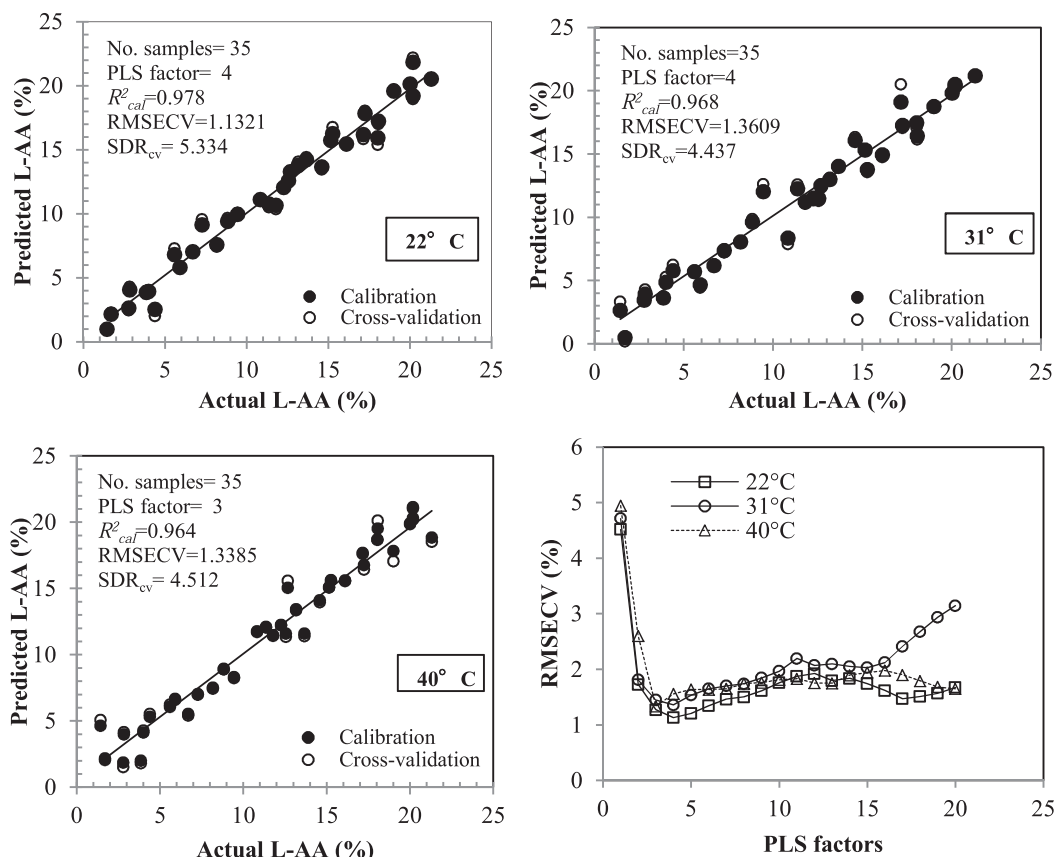


Fig. 4. The scatter plot of the best local calibration model for L-AA determination and the plot of PLS factors versus RMSECV at 22, 31 and 40 °C.

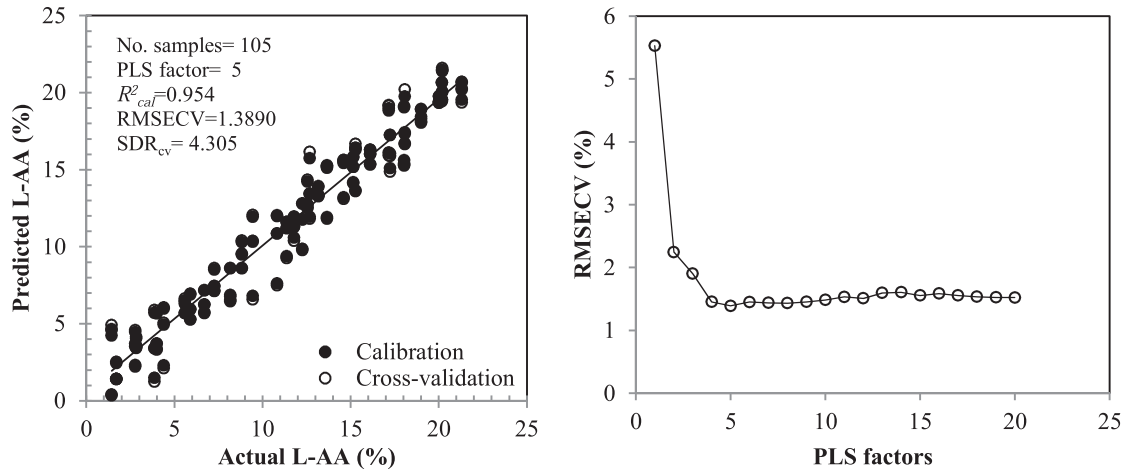


Fig. 5. The scatter plot of the best global calibration model for L-AA determination and the plot of PLS factors versus RMSECV using combination of calibration sample set at 22, 31 and 40 °C.

calibration model. To evaluate the influence of different spectral pre-processing methods, several spectral pre-processing methods were employed, including smoothing (moving average and Savitzky–Golay), differentiation (Savitzky–Golay and Norris), standard normal variate (SNV) and multiplicative scatter correction (MSC) (data are not shown). Finally, the best pre-processed spectra were obtained with Savitzky–Golay (SG) smoothing for 9 segments. The results are presented in Table 3. The global calibration models were quite good for all combinations. High  $R^2_{cal}$  and low RMSECV values were obtained for all the global calibration models. The  $SDR_{cv}$  values were also more than 3 (Table 3). In general, the global calibration models have higher PLS factors compared to those of the local calibration models at 22, 31 and 40 °C (Table 3). This means that the complexity of combined sample sets lead to an increasing number of PLS factors in the global calibration model, which is in agreement with previous reports (Segtnan et al., 2005).

Table 4

The performance of the calibration model with and without temperature compensation for L-AA prediction using uncombined and combined prediction sample set using the best calibration model of Savitzky–Golay smoothing spectra in the range 20–450  $cm^{-1}$ .

Calibration model	Prediction sample set temperature	$R^2_{pred}$	SEP	Bias	RMSEP	$SDR_{pred}$
22 °C	22 °C	0.954	1.319	0.049	1.280	4.668
Local calibration	31 °C	0.874	2.128	6.187	6.522	0.916
	40 °C	0.912	1.860	12.182	12.314	0.485
31 °C	22 °C	0.943	1.615	-3.730	4.046	1.477
	31 °C	0.891	1.994	-0.490	1.996	2.994
40 °C	40 °C	0.931	1.593	4.156	4.434	1.348
	22 °C	0.954	1.290	-7.487	7.591	0.787
Local calibration	31 °C	0.891	2.004	-4.077	4.517	1.323
	40 °C	0.960	1.258	-0.101	1.224	4.880
22 and 31 °C	22 °C	0.952	1.340	0.162	1.310	4.562
	31 °C	0.908	1.824	-0.569	1.858	3.216
Global calibration	40 °C	0.947	1.421	0.289	1.408	4.244
	22 °C	0.956	1.245	0.134	1.216	4.914
31 and 40 °C	31 °C	0.906	1.860	-0.622	1.908	3.132
	40 °C	0.954	1.284	-0.205	1.262	4.735
22 and 40 °C	22 °C	0.954	1.271	0.051	1.234	4.843
	31 °C	0.902	1.938	-0.711	2.011	2.972
Global calibration	40 °C	0.962	1.180	-0.134	1.152	5.187
	22 °C	0.954	1.272	0.124	1.240	4.820
22, 31 and 40 °C	22 °C	0.906	1.861	-0.710	1.940	3.080
	40 °C	0.956	1.245	-0.053	1.209	4.942

Compared to the local calibration models, the global calibration models were poorer in quality, with higher RMSECV and lower  $SDR_{cv}$  values. It is interesting that the global calibration model at 22 and 40 °C with 70 samples resulted in a higher  $SDR_{cv}$  value compared to that of 22, 31 and 40 °C combination with 105 samples. It should be noted that both these models have the same temperature range. A plot of PLS factors versus RMSECV and a scatter plot of the global calibration model for L-AA determination at 22, 31 and 40 °C (combination of three different temperatures) are depicted in Fig. 5. Based on Fig. 5, the optimal number of PLS factor is 5.

3.4. Evaluation of sample temperature on model performance using local and global calibration model

To evaluate the performance of the best local and global calibration models, a prediction of L-AA concentration using an external sample set was conducted. The results are presented in Table 4. Using the best local calibration model at 22, 31 and 40 °C, the prediction results for the prediction sample set at each temperature were excellent, with a low RMSEP and a high  $SDR_{pred}$ . However, the prediction results at different temperatures were not

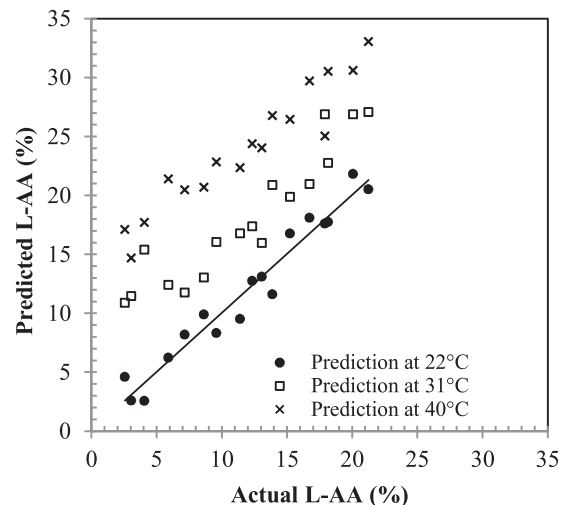


Fig. 6. Scatter plot of actual versus predicted L-AA for prediction sample set at 22, 31 and 40 °C predicted by using the best local calibration at 22 °C.

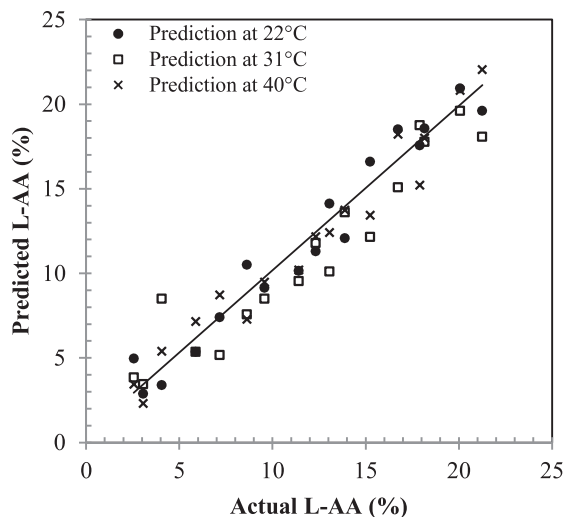


Fig. 7. Scatter plot of actual versus predicted L-AA for prediction sample set at 22, 31 and 40 °C predicted by using the best global calibration using combination of three different temperatures of 22, 31 and 40 °C.

as accurate as those obtained by the prediction sample set at the same temperature. The bias and SEP were significantly increased when the best local calibration at 22, 31 and 40 °C were used for prediction of samples measured at different temperatures; this resulted in high RMSEP values (Table 4). It can be concluded from this that the local calibration model for L-AA determination are sensitive to sample temperature deviations. When the temperature between the prediction samples and the calibration model increased, a larger predictive error of the L-AA was observed ( $SDR_{pred}$ ). This effect was found for all local calibration models at 22, 31 and 40 °C.

From Table 4 it is also clear that the effect of temperature difference on model performance is largest, in terms of prediction bias but not SEP, when the calibration and prediction spectral data were acquired at different temperatures, which is in agreement with previous reports (Miyamoto and Kitano, 1995; Sanchez et al., 2003; Guthrie and Walsh, 1999; Golic and Walsh, 2006). The effect of sample temperature differences between the calibration and prediction is visualized for the best local calibration at 22 °C in Fig. 6. The prediction was least accurate for the largest temperature differences between the calibration and prediction samples. This error was mainly due to an underestimation of the L-AA.

From Table 4, we can see that compared to the local calibration models at 22, 31 and 40 °C, the global calibration models based on a combination of different temperatures resulted in better prediction results, with lower RMSEP and higher  $SDR_{pred}$  values for all prediction samples at 22, 31 and 40 °C. When the bias predictions were significantly decreased, this resulted in lower RMSEPs. The reason for this increase in the robustness of the global calibration model is the incorporation of more sampled temperatures in the calibration sample set, thereby increasing the resistance against small measurement deviations. The effect of the increased model robustness for the global calibration model in regards to temperature variations of the prediction samples is depicted in Fig. 7. It can be seen that biases or other errors are no longer seen.

The use of global calibration models which are capable of compensating for temperature variations in the prediction samples is promising from a practical perspective for L-AA determination. The prediction results of the global calibration models were even better than those of the local calibration models established at the same temperature. For example, for the prediction sample at 22 °C,

when it was predicted using a local calibration model established at 22 °C, resulted in  $SDR_{pred} = 4.668$ . While a higher  $SDR_{pred} = 4.820$  results were obtained when predicted using the global calibration models. Similar results were also found for prediction results at 31 and 40 °C, which is in agreement with previous reports (Guthrie and Walsh, 1999; Sanchez et al., 2003; Kawano et al., 1995; Miyamoto and Kitano, 1995). This result shows that with a broader temperature range for the calibration samples, more accurate predictions can be obtained. Previous studies, Peirs et al. (2003) and Kawano et al. (1995) have also shown that calibration models developed over a broad range of sample temperatures provided a more robust measurement of soluble solids of apples and peaches, respectively.

#### 4. Summary and conclusions

To summarize, we measured L-AA spectral data with broad spectrum THz spectroscopy at three different temperatures (22, 31 and 40 °C), and investigated the effect of sample temperature on model performance for L-AA determination. We established a global calibration model that can compensate for sample temperature variations between 22 and 40 °C. The prediction results using this global calibration model are improved significantly with low bias. Predictions for this model had a lower RMSEP and a high  $SDR_{pred}$  value compared to that of the local calibration models. It is shown that a global calibration model with temperature correction can handle variations in sample temperature effectively and provide an effective method for compensating for temperature variations in L-AA determination using THz spectroscopy.

#### Acknowledgment

The authors would like to gratefully acknowledge Dr. Garry J Piller, professor of 30G programs at Graduate School of Agriculture, Kyoto University for his suggestion, comments, and valuable discussion and for proof reading of the manuscript. The authors would like to thank Directorate General of Higher Education (DGHE/DIKTI), Ministry of Education and Culture, Indonesia, Lampung University and Lampung State Polytechnic for supporting the scholarship.

#### References

- Al-Holy MA, Lin M, Cavinato AG, Rasco BA. The use of Fourier transform infrared spectroscopy to differentiate *Escherichia coli* O157:H7 from other bacteria inoculated into apple juice. *Food Microbiol* 2006;23(2):162–8.
- Al-Qadiri HM, Lin MS, Cavinato AG, Rasco BA. Fourier transform infrared spectroscopy, detection and identification of *Escherichia coli* O157:H7 and *Alicyclobacillus* strain in apple juice. *Int J Food Microbiol* 2006;111(1):73–80.
- Burdurlu HS, Koca N, Karadeniz F. Degradation of vitamin C in citrus juice concentration during storage. *J Food Eng* 2006;74(2):211–6.
- Cen HY, He Y, Huang M. Measurement of soluble solids contents and pH in orange juice using chemometrics and vis-NIRS. *J Agric Food Chem* 2006;54(20):7437–43.
- Centner V, Massart D, de Noord OE, de Jong S, Vandeginste BM, Sterna C. Elimination of uninformative variables for multivariate calibration. *Anal Chem* 1996;68(21):3851–8.
- Clement A, Dorais M, Vernon M. Nondestructive measurement of fresh tomato lycopene content and other physicochemical characteristics using visible-NIR spectroscopy. *J Agric Food Chem* 2008;56:9813–8.
- Duarte IF, Barros A, Delgadillo I, Almeida C, Gil AM. Application of FTIR spectroscopy for the quantification of sugars in mango juice as a function of ripening. *J Agric Food Chem* 2002;50(11):3104–11.
- Golic M, Walsh KB. Robustness of calibration models based on near infrared spectroscopy for the in-line grading of stone fruit for total soluble solids content. *Anal Chim Acta* 2006;555:286–91.
- Guthrie J, Walsh K. Influence of environmental and instrumental variables on the non-invasive prediction of Brix in pineapple using near infrared spectroscopy. *Aust J Exp Agric* 1999;39(1):73–80.

- Ikedo T, Matsushita A, Tatsuno M, Minami Y, Yamaguchi M, Yamamoto K, et al. Investigation of inflammable liquids by terahertz spectroscopy. *Appl Phys Lett* 2005;87:034105-1–034105-3.
- Jepsen PU, Jensen JK, Moller U. Characterization of aqueous alcohol solutions in bottles with THz reflection spectroscopy. *Opt Express* 2008;16(13):9318–31.
- Kawano S, Abe H, Iwamoto H. Development of a calibration equation with temperature compensation for determining the Brix value in intact peaches. *J Near Infrared Spectrosc* 1995;3:211–8.
- Kelly JD, Downey G. Detection of sugar adulterants in apple juice using Fourier transform infrared spectroscopy and chemometrics. *J Agric Food Chem* 2005;53(9):3281–6.
- Lanza E, Li BW. Application for near infrared spectroscopy for predicting the sugar content of fruit juices. *J Food Sci* 1984;49(4):995–8.
- Leon L, Kelly JD, Downey G. Detection of apple juice adulteration using near infrared transreflectance spectroscopy. *Appl Spectrosc* 2005;59(5):593–9.
- Liu Y, Sun X, Zhou J, Zhang H, Yang C. Linear and nonlinear multivariate regressions for determination sugar content of intact Gannan navel orange by vis-NIR diffuse reflectance spectroscopy. *Math Comput Model* 2010;51:1438–43.
- Miyamoto K, Kitano Y. Non-destructive determination of sugar content in Satsuma mandarin fruit by near infrared transmittance spectroscopy. *J Near Infrared Spectrosc* 1995;3:227–37.
- Ogawa Y, Cheng L, Hayashi S, Fukunaga K. Attenuated total reflection spectra of aqueous glycine in the terahertz region. *IEICE Electron Express* 2009;6(2):117–21.
- Peirs A, Scheerlinck N, Nicolai BM. Temperature compensation for near infrared reflectance measurement of apple fruit soluble solids contents. *Postharvest Biol Technol* 2003;30:233–48.
- Ros-Chumillas M, Belissario Y, Iguaz A, López A. Quality and shelf life of orange juice aseptically packaged in PET bottles. *J Food Eng* 2007;79(1):234–42.
- Rønne C, Thrane L, Astrand P, Wallqvist A, Mikkelsen KV, Keiding SR. Investigation of the temperature dependence of dielectric relaxation in liquid water by THz reflection spectroscopy and molecular dynamics simulation. *J Chem Phys* 1997;107(14):5319–31.
- Rønne C, Astrand P, Keiding SR. THz spectroscopy of liquid H<sub>2</sub>O and D<sub>2</sub>O. *Phys Rev Lett* 1999;82(14):2888–91.
- Rønne C, Keiding SR. Low frequency of liquid water using THz-time domain spectroscopy. *J Mol Liq* 2002;101(1–3):199–218.
- Sanchez NH, Lurol S, Roger JM, Maurel VB. Robustness of model based on NIR spectra for sugar content prediction in apples. *J Near Infrared Spectrosc* 2003;11(2):97–107.
- Segtnan VH, Mevik B, Isaksson T, Naes T. Low-cost approaches to robust temperature compensation in near infrared calibration and prediction situations. *Appl Spectrosc* 2005;59(6):816–25.
- Suhandy D, Suzuki T, Ogawa Y, Kondo N, Naito H, Ishihara T, et al. A quantitative study for determination of glucose concentration using attenuated total reflectance terahertz (ATR-THz) spectroscopy. *Eng Agric Environ Food EAEF* 2012a;5(3):90–5.
- Suhandy D, Yulia M, Ogawa Y, Kondo N. L-Ascorbic acid prediction in aqueous solution based on FTIR-ATR terahertz spectroscopy. *Eng Agric Environ Food EAEF* 2012b;5(4):152–8.
- Swierenga H, Wulfert F, de Noord OE, de Weijer AP, Smilde AK, Buydens LMC. Development of robust calibration models in near infra-red spectrometric applications. *Anal Chim Acta* 2000;411:121–35.
- Sørensen LK, Dalsgaard S. Determination of clay and other soil properties by near infrared spectroscopy. *Soil Sci Soc Am J* 2005;69:159–67.
- Valente M, Leardi R, Self G, Luciano G, Pain JP. Multivariate calibration of mango firmness using vis/NIR spectroscopy and acoustic impulse method. *J Food Eng* 2009;94:7–13.
- Wulfert F, Kok WT, de Noord OE, Smilde AK. Correction of temperature-induced spectral variation by continuous piecewise direct standardization. *Anal Chem* 2000;72(7):1639–44.
- Wulfert F, Kok WT, Smilde AK. Influence of temperature on vibrational spectra and consequences for the predictive ability of multivariate models. *Anal Chem* 1998;70(9):1761–7.
- Yada H, Nagai M, Tanaka K. Origin of the fast relaxation component of water and heavy water revealed by terahertz time-domain attenuated total reflection spectroscopy. *Chem Phys Lett* 2008;464:166–70.
- Zelmann HR. Temperature dependence of the optical constant for liquid H<sub>2</sub>O and D<sub>2</sub>O in the far IR region. *J Mol Struct* 1995;350:95–114.